engineering proceedings

MDPI

Proceeding Paper

Durability and Gamma Shielding of MWCNT- and GNP-Modified Mortars Under Wet–Dry Sulfate Cycling †

Fatima I. AlHamadi [1,2] and Ahmed K. AlKaabi [1,2,*]

[1] Department of Mechanical and Nuclear Engineering, Khalifa University of Science and Technology, Abu Dhabi P.O. Box 127788, United Arab Emirates; 100060569@ku.ac.ae
[2] Emirates Nuclear Technology Center, Khalifa University of Science and Technology, Abu Dhabi P.O. Box 127788, United Arab Emirates
* Correspondence: ahmed.alkaabi@ku.ac.ae
† Presented at the 15th Central European Congress on Concrete Engineering (CCC2026), Vodice, Croatia, 5–7 October 2026.

Abstract

This study examines the effect of wet and dry sulfate cycling on the durability and gamma-ray shielding of carbon-based nano-modified mortars for nuclear infrastructure in arid environments. Ordinary mortar was compared with 0.05% multi-walled carbon nanotubes (MWCNTs; designated CN5), 0.05% graphene nanoplatelets (GNPs; designated G5) and 0.10% GNP(designated G10) mortars before and after 4 months of cyclic sulfate exposure. After 4 months, the compressive strength remained stable or increased, while electrical resistivity decreased by 37–54%, showing transport-related degradation. G10 achieved the highest flexural strength of 12.7 MPa and showed 35% higher attenuation than the ordinary mortar at 1173 keV. G10 provided the best combined durability and shielding performance.

Keywords: wet–dry sulfate cycling; graphene nanoplatelets; carbon nanotubes; gamma-ray shielding; durability

1. Introduction

Concrete is widely used in nuclear power plants, spent fuel storage facilities, radioactive waste containment systems and biological shielding structures because it provides both structural support and radiation attenuation. In these applications, concrete is exposed to harsh environmental and operational conditions that gradually affect both durability and shielding performance. This issue is critical in arid coastal regions such as the United Arab Emirates (UAE), where nuclear infrastructure is exposed to elevated temperatures, sulfate attacks, saline environments and repeated wetting and drying conditions. Although arid regions are characterized by low rainfall and high evaporation, concrete structures in coastal areas may still undergo intermittent wetting through sulfate-bearing groundwater, saline moisture, high humidity, fog, dew formation, condensation, splash exposure or periodic water contact. Subsequent drying at elevated temperatures promotes moisture loss and sulfate salt crystallization within the pore structure [1].

Wet–dry exposure occurs in real-world service environments where concrete structures experience alternating contact with sulfate-containing water followed by evaporation and drying [1,2]. Examples include splash and tidal zones, groundwater fluctuation regions, surface condensation zones and partially buried concrete structures in hot climates. In arid regions, high daytime temperatures accelerate moisture evaporation during drying periods, while sulfate-rich groundwater or saline moisture re-enters the pore structure during

Check for updates

Academic Editors: Josip Galić, Jelena Bleiziffer, Davor Andrić and Vita Varezić

Published: 3 November 2026

Copyright: © 2026 by the authors. Licensee MDPI, Basel, Switzerland. This article is an open access article distributed under the terms and conditions of the Creative Commons Attribution (CC BY) license.

wetting stages [3]. Compared with continuous immersion, wet–dry sulfate cycling is more aggressive because the wet stage promotes sulfate ingress, while the drying stage accelerates sulfate crystallization and the crystallization pressure within pores and cracks [2,4].

A sulfate attack is a deterioration mechanism that affects cement-based materials. Sulfate ions react with calcium aluminate phases and calcium hydroxide to form ettringite and gypsum [1,3]. These products initially fill pores and densify the matrix, which can temporarily improve compressive behavior. Their continued formation generates expansive stresses and internal cracking. Previous studies have reported that sulfate exposure initially increases compressive strength due to pore refinement and reduced transport resistance resulting from microcrack formation and the development of pore connectivity [1,2]. Under wet–dry cycling, repeated dissolution and crystallization intensify the internal damage [2,4].

Carbon-based nanomaterials have recently attracted attention for their potential to improve the performance of cementitious materials. Multi-walled carbon nanotubes (MWCNTs) improve stress transfer and crack bridging because of their high aspect ratio and mechanical strength [5,6]. The layered morphology and high surface area of graphene nanoplatelets (GNPs) help refine the pore structure and restrict crack propagation [7,8]. A recent study on graphene family materials reported improvements in microstructure, mechanical performance and durability indicators of cement-based composites, where their effect depended on dispersion quality and dosage [8]. Previous studies focused on mechanical or durability properties under normal curing or full immersion conditions [5–14]. But limited studies investigated the combined influence of wet–dry sulfate exposure and gamma-ray shielding behavior.

Radiation shielding concrete performance is influenced by the density, elemental composition, aggregate type, porosity, moisture condition and internal cracking [14–18]. Environmental degradation alters the pore structure, crack connectivity, moisture distribution and the effective photon interaction path, which changes the attenuation behavior over time [14,15,17,19]. Our previous work showed that sulfate exposure combined with elevated temperatures change both the durability indicators and gamma attenuation performance of blended cement mortars, which confirms that the shielding behavior should be assessed after environmental exposure rather than only in the unexposed state [17]. The wet–dry sulfate cycling effect on CNT- and GNP-modified mortars is less understood. This gap is important for nuclear-related infrastructure in arid coastal regions where concrete must maintain both resistance to degradation and radiation attenuation capacity.

The novelty of this study lies in evaluating the combined effect of wet–dry sodium sulfate cycling on both the durability and gamma shielding performance of carbon-based nano-modified mortars for radiation shielding applications. Unlike previous studies that mainly focused on mechanical behavior or unexposed shielding properties, this work will investigate the evolution of mechanical, transport-related, physical and attenuation properties under cyclic thermo-chemical exposure conditions representative of arid environments, such as the UAE.

The ordinary mortar (O) was compared with mortars containing 0.05% multi-walled carbon nanotubes (CN5), 0.05% graphene nanoplatelets (G5), and 0.10% graphene nanoplatelets (G10). The mortars were evaluated before exposure and after 4 months of cyclic sulfate exposure consisting of 8 h of immersion in a sulfate solution at 25 °C followed by 16 h of drying at 50 °C. The investigated properties included compressive strength, flexural strength, ultrasonic pulse velocity (UPV), density, electrical resistivity (ER), and gamma-ray linear attenuation coefficients at 662, 1173, and 1333 keV.

https://doi.org/10.3390/engproc2026161033

2. Materials and Methods

2.1. Materials and Mix Design

Type I ordinary Portland cement (OPC), supplied by Arabian Cement Industry LLC (Abu Dhabi, UAE), was used as the primary binder material in all mortar mixtures. Dune sand and crushed sand were used as fine aggregates and they were sourced from the Western Bainoona Group (Abu Dhabi, UAE). Desalinated water was used for mixing, nanomaterial dispersion and curing throughout the experimental program. A 0.4 water-to-binder ratio was maintained for all mortars. A polycarboxylate-based high-range water-reducing admixture (HRWRA; SikaPlast®-888 AE, Sika UAE L.L.C., Dubai, UAE) was incorporated to improve workability and assist nanomaterial dispersion.

Two carbon-based nano-additives were investigated: MWCNTs (Applied NanoStructured Solutions, LLC, Baltimore, MD, USA) and GNPs (PureGRAPH® 50, First Graphene Ltd., Henderson, WA, Australia). MWCNTs were selected because of their crack-bridging capability and high aspect ratio [5,6,10,11], while GNPs were selected because of their ability to improve matrix densification and pore refinement [7,8,12–14].

Four mortar mixtures were prepared using the mix design in Table 1:

- O: Ordinary mortar (O);
- CN5: 0.05 wt.% MWCNT-modified mortar;
- G5: 0.05 wt.% GNP-modified mortar;
- G10: 0.10 wt.% GNP-modified mortar.

Table 1. Mix design of the investigated mortar samples (per batch) in grams.

Sample ID	Cement	Dune Sand	Crushed Sand	Water	HRWRA	Nano-Additives
O	495	302.5	928	192	6	0
CN5	495	302.5	928	192	6	0.248
G5	495	302.5	928	192	6	0.248
G10	495	302.5	928	192	6	0.495

The selected CNT and GNP dosages were based on previous studies reporting that low nano-carbon contents generally provide the best balance between mechanical enhancement, dispersion quality and workability [6,9–13]. Previous investigations have shown that low nano-additive contents can improve mechanical performance, transport resistance and matrix behavior, while higher dosages or inadequate dispersion may reduce workability and lead to nanomaterial agglomeration, which can limit the expected improvement in mortar performance [6,9–13], as summarized in Table 2. The GNPs used in this study were PureGRAPH® 50, supplied as black powder with a median particle size of 50.3 µm and a tapped density of 0.177 g/cm^3. Raman analysis showed D, G and 2D peaks at 1350.1, 1575.6 and 2696.9 cm^{-1}, respectively, with a D/G ratio of 0.339. The MWCNTs had a reported carbon nanotube content greater than 93%, with fiberglass content below 1%, polyethylene glycol (PEG) content below 6% and a length range of 1–500 µm.

Table 2. Literature-based justification for CNT and GNP dosage selection.

Reference	Nanomaterial	Effective Dosage	Findings
Hassan et al. [6]	CNT	0.05 wt.%	0.05% CNT as the optimum content for improving compressive, tensile, and flexural strength
Maqsood et al. [9]	MWCNT	0.05 wt.%	improved transport/chloride resistance using low CNT dosage
Arrechea et al. [10]	MWCNT	0.01–0.05 wt.%	improved mechanical compression behavior of cement-based materials with MWCNT addition

Table 2. *Cont.*

Reference	Nanomaterial	Effective Dosage	Findings
Zhou et al. [12]	GNP	0.05–0.10 wt.%	low GNP dosages as part of dispersion/ performance optimization
Ge et al. [13]	GNP	0.05–0.10 wt.%	dosage-dependent effects of GNPs on workability, setting, strength, and related properties

2.2. Specimen Preparation and Wet–Dry Exposure

Before mixing, water, HRWRA and nano-additives were premixed and dispersed using a Vibra-Cell probe sonicator (Sonics & Materials, Inc., Newtown, CT, USA) for 30 min at 40% amplitude in a pulsed mode of 5 s ON followed by 2 s OFF. The temperature of the nano-suspension was not monitored during sonication, although a temperature increase due to ultrasonic energy input was expected. The resulting nano-suspension was then added during mortar mixing. The control mortar was prepared using the same procedure but without nano-additives, ensuring that any performance changes were mainly related to the nano-carbon modification.

The mortars were cast into a cube (5 × 5 × 5 cm) for compressive strength, prism (16 × 4 × 4 cm) for flexural strength, UPV and ER, and slab (1 × 10 × 10 cm) for density and gamma-ray attenuation measurements. After casting, the mortars were demolded after 24 h and water cured for 28 days before chemical exposure. After curing, mortars were subjected to wet and dry sodium sulfate cycling as an accelerated laboratory exposure condition relevant to concrete structures that experience intermittent sulfate-bearing moisture and elevated temperature drying in arid coastal environment. Each cycle consisted of 8 h immersion in sodium sulfate solution at 25 °C followed by 16 h drying at 50 °C in oven. The drying stage simulated elevated daytime temperatures and evaporation conditions commonly experienced in arid environments. Compared with full immersion, wet–dry sulfate cycling accelerates sulfate ingress, salt crystallization and internal expansive reactions due to repeated moisture transport and crystallization pressure development [1–4]. The exposure duration in this study was 4 months. Measurements were conducted before exposure (0 M) and after exposure (4 M).

2.3. Testing Methods

Before and after 4 months of wet–dry cyclic exposure, characterization tests were performed. Compressive strength was examined in accordance with ASTM C109 /C109M-24 [20]. Flexural strength was assessed in accordance with ASTM C348 [21] under three-point loading. UPV measurements were conducted using ASTM C597 [22] to evaluate internal structural integrity and wave transmission behavior. ER measurements were conducted using the four-probe Wenner method to assess transport-related durability behavior and pore connectivity after sulfate exposure, adapted from AASHTO T358 standards [23]. Bulk density was determined from the mortar mass to volume ratio.

Gamma-ray shielding performance was evaluated using the linear attenuation coefficient (μ). Measurements were conducted using Cs-137 and Co-60 radioactive sources at photon energies of 662, 1173 and 1333 keV. The transmitted gamma intensity through the mortar slabs was measured using a high-purity germanium (HPGe) detector system (model BE2825, Canberra Industries, Inc., Meriden, CT, USA). μ was determined using Beer–Lambert's law:

$$I = I_0\, e^{-\mu x} \quad (1)$$

where I_0 is the incident photon intensity, I is the transmitted photon intensity, x is the slab thickness and μ is the linear attenuation coefficient. Figure 1 presents the radioactive

gamma-ray sources and HPGe detector system used for the attenuation measurements. The attenuation measurements were conducted before exposure and after 4 months of wet–dry sulfate cycling to evaluate the influence of environmental degradation on shielding performance.

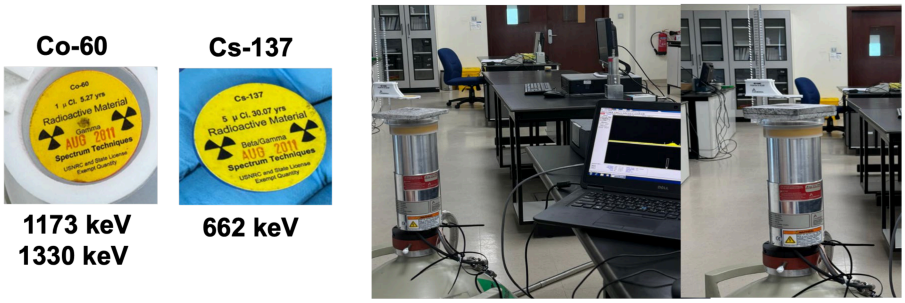


Figure 1. Gamma-ray attenuation measurement setup: (**a**) Co-60 and Cs-137 radioactive sources and (**b**) high-purity germanium (HPGe) detector system used for transmitted gamma-ray intensity measurements.

Unless otherwise stated, the reported results represent the mean ± standard deviation of three replicate specimens for each mixture and exposure condition.

3. Results and Discussion

3.1. Mechanical Performance Under Wet–Dry Sulfate Cycling

The compressive and flexural strength results after 4 months of wet–dry sulfate exposure are presented in Figure 2. The results indicate that cyclic sulfate exposure produced two competing mechanisms: pore filling and internal degradation. During wetting, sulfate ions ingress into the pore system and react with cement hydration products, leading to the formation of ettringite and gypsum [1,3]. These products can partially fill pores and temporarily densify the matrix. During drying, water evaporation promotes sulfate crystallization, crystallization pressure and moisture gradient stresses, which can initiate internal microcracks [1,2,4]. Compressive strength increased after exposure. The compressive strength of the ordinary mortar increased 22% from 43 to 53 MPa. CN5 recorded the highest post-exposure compressive strength of 65 MPa. The compressive strengths of G5 and G10 increased by 8% and 3%, respectively. The larger relative increase in the ordinary mortar indicates stronger pore-filling effects in the unmodified matrix, while the smaller increase in nano-modified mortars suggests that these mixes already had a more refined initial structure before exposure.

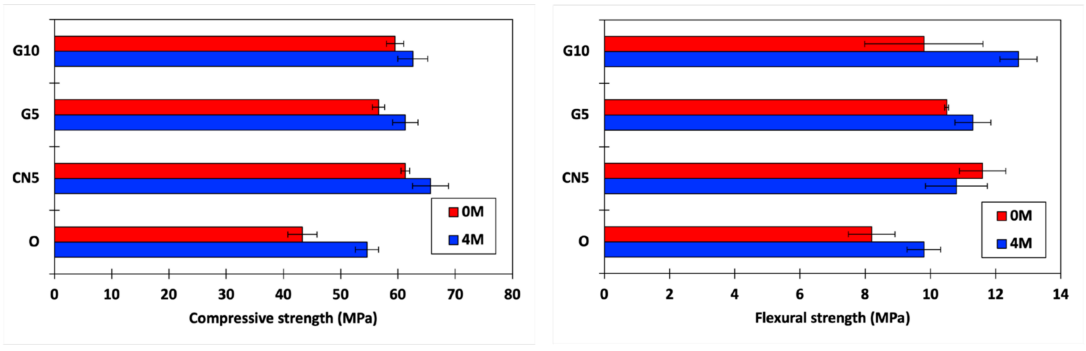


Figure 2. (**a**) Compressive strength and (**b**) flexural strength of ordinary and nano-modified mortars before exposure (0 M) and after 4 months of wet–dry sodium sulfate cycling.

Flexural strength showed a mix-dependent response. G10 exhibited the highest post-exposure flexural strength of 12.7 MPa, that is 30% higher than the ordinary mortar after exposure, and a 30% increase relative to its 0 M value, indicating improved crack resistance under cyclic sulfate exposure. The flexural strength of G5 increased by 8%, and the ordinary mortar increased the flexural strength by about 20%. The flexural strength of CN5 decreased by 7%, despite maintaining the greatest compressive strength. This confirms that compressive behavior alone does not fully represent the damage caused by wet–dry sulfate cycling, especially because flexural strength is more sensitive to crack initiation and propagation. The improved flexural behavior of G10 is related to the crack-bridging effect and crack growth restriction provided by GNPs [7,8,12–14].

3.2. Electrical Resistivity Behavior

ER before and after 4 months of wet–dry sulfate cyclic exposure is illustrated in Figure 3. ER was the most sensitive durability indicator, decreasing substantially for all mixes after exposure. The ER of the ordinary mortar decreased by 43%, while the ER of CN5 showed the greatest reduction of 54%. The ER of G5 and G10 showed reductions of 37% and 40%, respectively. The 54% reduction in the ER of CN5 was about 1.45 times greater than the reduction observed for G5, indicating higher sensitivity to cyclic sulfate-induced transport deterioration. The reduction in ER was caused by the wet–dry sulfate cycling mechanism. During wetting, sulfate ions entered the pore system and started chemical reactions that produced sulfate reaction products, such as ettringite and gypsum [1,3]. During drying, sulfate reaction products inside the pores generate crystallization pressure and promote cracking, thereby widening transport pathways [1,2,4]. ER decreased as connected pores and microcracks controlled ionic transport, despite increased compressive strength from pore filling. The increase in compressive strength together with the 37–54% reduction in ER indicates that wet–dry sulfate cycling may improve the apparent load-bearing capacity at the investigated exposure stage while increasing transport-related deterioration. G5 and G10 maintained better ER than the ordinary mortar and CN5, suggesting that GNP incorporation helped reduce the development of connected damage pathways under cyclic sulfate exposure.

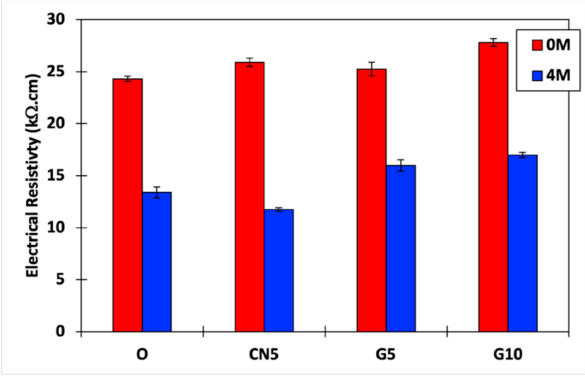


Figure 3. Electrical resistivity of ordinary and nano-modified mortars before exposure (0 M) and after 4 months of wet–dry sulfate cycling.

3.3. Ultrasonic Pulse Velocity and Density Response

UPV and density results are shown in Figure 4. UPV remained relatively stable for most mixes, but the response differed depending on the nano-modification. The ordinary mortar showed a UPV increase of 2.9%, while G10 remained unchanged with a 0.5% increase. G5 showed a small decrease in UPV of 2.3%. These limited changes suggest that sulfate product depositions have partially filled pores and maintained wave transmission through

the matrix. CN5 showed the largest UPV reduction of 8.7%, indicating increased internal discontinuities and microcrack formation. This trend agrees with the reduction in flexural strength and large ER loss, suggesting that wet–dry sulfate cycling caused more pronounced internal damage in the MWCNT-modified mortar. The repeated crystallization of sulfate salts during drying can reduce the continuity of the solid skeleton and weaken ultrasonic wave propagation [1,2,4].

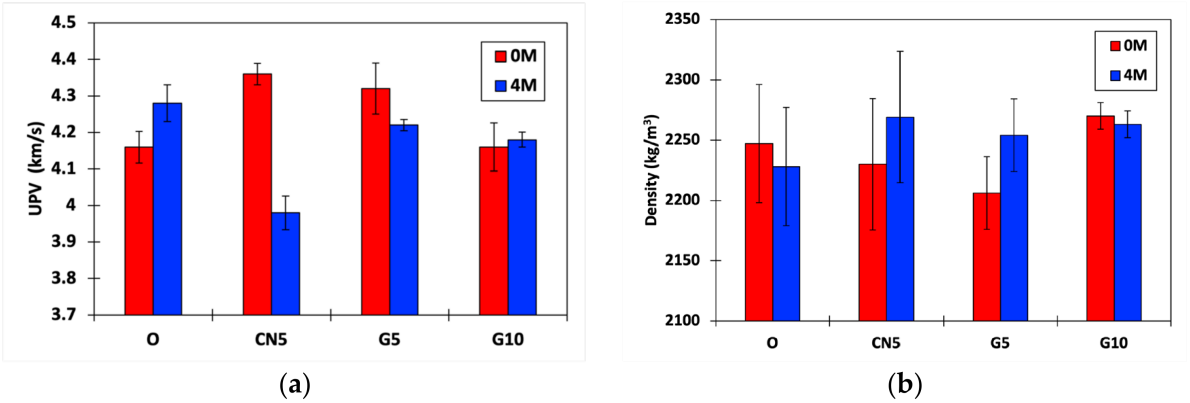


Figure 4. (**a**) UPV and (**b**) bulk density of ordinary and nano-modified mortars before exposure (0 M) and after 4 months of wet–dry sulfate cycling.

Density changes were small for all mixes, ranging from a 0.8% decrease in the ordinary mortar to a 2.2% increase in G5. The density of CN5 showed a 1.7% increase, and the density of G10 showed a −0.3% decrease, respectively, which is related to the sulfate product deposition within pores. G10 showed only a minor density reduction of 0.3%, while the ordinary mortar decreased the density by 0.8%. These limited density changes indicate that the main effect of wet–dry sulfate exposure was not a bulk mass change but the modification of pore connectivity and the internal microstructure.

3.4. Gamma-Ray Shielding Performance

μ results are summarized in Figure 5. For all mixes, μ decreased with increasing photon energy, which is expected because higher-energy photons have a lower interaction probability with matter [5,16]. Radiation shielding performance in concrete depends mainly on density, composition, thickness and internal defects [15,16]. After wet–dry sulfate exposure, G10 showed the strongest shielding response. At 662 keV, G10 increased μ from 0.223 to 0.240 cm^{-1}, showing an 8% increase in μ. At 1173 keV, G10 increased μ from 0.169 to 0.210 cm^{-1}, corresponding to a 24% increase in μ. At 1333 keV, μ increased 7% from 0.166 to 0.178 cm^{-1}. Under the same wet–dry condition, the attenuation coefficient of G10 at 1173 keV was 35% higher than the ordinary mortar. CN5 showed attenuation reductions after exposure, with decreases of 12%, 5% and 14% at 662, 1173 and 1333 keV, respectively. This agrees with its reductions in flexural strength, UPV and ER, suggesting that microcracking reduced the effective shielding structure. G5 showed stable shielding behavior with changes close to zero at the investigated energies.

The improved attenuation response of G10 was linked to the combined effect of the improved microstructural stability, better crack resistance and partial pore filling by sulfate reaction products [1,3,7,8]. The simultaneous ER decrease and μ improvement in G10 shows that transport durability and radiation shielding do not always follow the same trend. ER is mainly controlled by connected ionic pathways, while μ depends on the density, the composition and the effective photon interaction path [15–18]. Therefore, wet–dry sulfate

exposure can reduce transport resistance while maintaining or improving attenuation if matrix densification and pore filling dominate the shielding response.

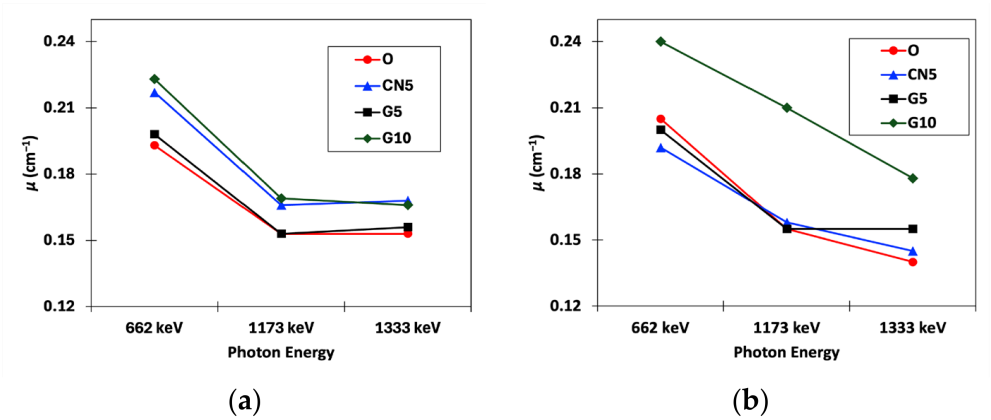


Figure 5. μ of ordinary and nano-modified mortars at different photon energies (**a**) before exposure (0 M) and (**b**) after 4 months of wet–dry sulfate cycling.

3.5. Integrated Durability and Shielding Assessment

The integrated percentage change plot in Figure 6 shows that the investigated performance indicators did not respond uniformly to wet–dry sulfate cycling. Mechanical properties improved, while ER decreased significantly. For example, the ordinary mortar showed a 22% increase in compressive strength, but its ER decreased by 43%. Similarly, CN5 maintained the highest compressive strength after exposure, but it showed the largest ER loss, the largest UPV reduction and attenuation losses at all investigated energies. These results confirm that compressive strength alone can underestimate the extent of the internal deterioration caused by cyclic sulfate exposure.

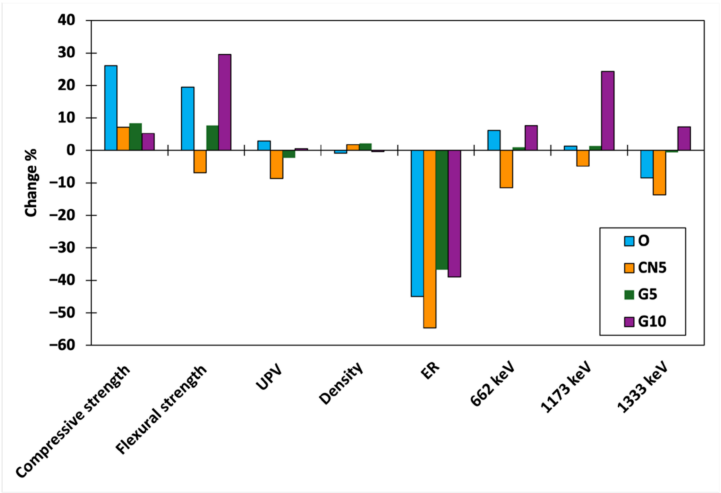


Figure 6. Integrated percentage changes in mechanical, transport, density, and gamma-ray shielding properties of ordinary and nano-modified mortars after 4 months of wet–dry sodium sulfate cycling, relative to the unexposed condition.

The relationship between the flexural strength change and μ variation is shown in Figure 7. Mixes with better flexural performance maintained better attenuation stability. G10 showed the strongest combined response, with a 30% flexural improvement and positive μ changes at all energies, while CN5 showed a 7% flexural reduction and attenuation losses of up to 14%. This suggests that crack resistance and microstructural stability are important

for maintaining shielding performance under wet–dry sulfate exposure. G10 provided the most balanced performance under cyclic sulfate exposure. Although CN5 achieved the highest compressive strength, G10 performed better for flexural behavior, shielding stability and overall durability. This is important for nuclear-related cementitious materials, where long-term performance depends on the structural durability and attenuation capacity together not compressive strength alone.

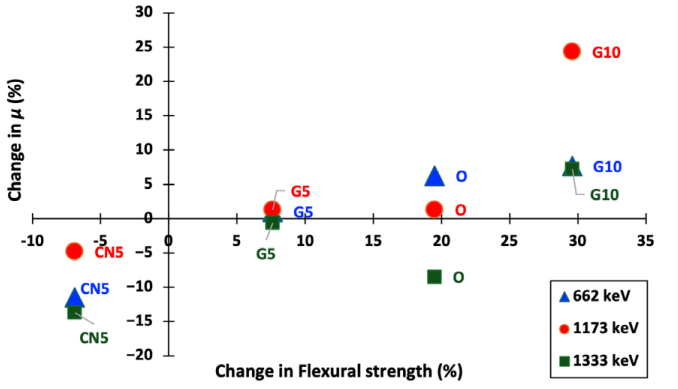


Figure 7. Relationship between flexural strength change and variation in μ at different photon energies after 4 months of sulfate wet–dry cycle.

4. Conclusions and Future Work

This study investigated the influence of wet–dry sodium sulfate cycling on the durability and gamma-ray shielding performance of ordinary and carbon-based nano-modified mortars for nuclear-related infrastructure in arid environments. The exposure condition consisted of repeated sulfate immersion and elevated temperature drying cycles designed to mimic the aggressive thermo-chemical conditions relevant to arid coastal regions.

The results showed that wet–dry sulfate exposure affected the investigated properties in different ways. Compressive strength increased after four months of exposure, because temporary pore filling by sulfate reaction products, including ettringite and gypsum, partially densified the matrix. However, under prolonged sulfate exposure, the continued formation of expansive products may cause cracking and subsequent strength loss.

However, transport-related properties were more sensitive to cyclic sulfate deterioration, indicating that the apparent improvement in compressive behavior did not necessarily represent improved overall durability. The response of the investigated mortars was mix-dependent. G10 showed the most balanced overall performance by maintaining favorable flexural behavior and positive attenuation coefficient changes, whereas CN5 exhibited the greatest reduction in ER and UPV.

This study shows that compressive strength alone is not enough to evaluate the long-term performance of cementitious materials exposed to cyclic sulfate environments. Durability indicators and shielding properties must be considered for nuclear infrastructure applications where structural integrity and radiation attenuation are both required throughout service life. This study illustrated that the GNP incorporation at 0.10 wt. % improved the combined durability and shielding response of mortars exposed to aggressive wet and dry sulfate environments, as is the case for arid coastal nuclear infrastructure, at the investigated 4-month exposure stage; however, longer-term exposure is required to establish sustained performance.

Future investigations should include longer exposure durations, microstructural characterization using X-ray diffraction (XRD) and scanning electron microscopy (SEM) analysis and irradiation-assisted degradation studies to better understand the combined influence

of sulfate attacks and radiation exposure on nano-modified cementitious materials. Additional studies on porosity evolution, drying temperature effects and alternative sulfate environments, such as magnesium sulfate and mixed chloride–sulfate exposure, are also recommended. Also, future studies should quantify fresh air content to assess the potential influence of nano-additive dispersion and mixing on the air volume of fresh mortars. Furthermore, extending the investigation to heavyweight shielding concretes containing barite, magnetite or hematite aggregates would provide a more representative assessment for nuclear shielding applications.

Author Contributions: F.I.A.: Methodology, conceptualization, writing—original draft, revision and editing final draft. A.K.A.: Funding acquisition, project administration, resources, validation, investigation, supervision, formal analysis, conceptualization, editing final draft and revision. All authors have read and agreed to the published version of the manuscript.

Funding: This research was funded by the Emirates Nuclear Technology Center (KU-ENTC), a collaboration amongst Khalifa University of Science and Technology, Emirates Nuclear Energy Company and the Federal Authority for Nuclear Regulation.

Institutional Review Board Statement: Not applicable.

Informed Consent Statement: Not applicable.

Data Availability Statement: The data will be made available upon reasonable request from the corresponding author.

Conflicts of Interest: The authors declare no conflicts of interest. The authors declare that they have no known competing financial interests or personal relationships that could have appeared to influence the work reported in this paper.

References

1. Zhang, C.; Li, J.; Yu, M.; Lu, Y.; Liu, S. Mechanism and Performance Control Methods of Sulfate Attack on Concrete: A Review. *Materials* **2024**, *17*, 4836. [CrossRef] [PubMed]
2. Qin, S.; Chen, C.; Zhang, M. Modeling of Concrete Deterioration under External Sulfate Attack and Drying–Wetting Cycles: A Review. *Materials* **2024**, *17*, 3334. [CrossRef] [PubMed]
3. Wang, Q.; Kunther, W.; Li, Y.; Visalakshi, T.; Gomasa, R.; Amroun, S.; De Souza, D.J.; Kasaniya, M.; Tole, I.; Li, X.; et al. Sulfate Attack Testing Approaches from Concrete to Cement Paste: A Review by RILEM TC 298-EBD. *Mater. Struct.* **2025**, *58*, 232. [CrossRef]
4. Shan, Z.-Q.; Yin, G.-J.; Wen, X.-D.; Miao, L.; Wang, S.-S.; Zuo, X.-B. Numerical Simulation on Transport-Crystallization-Mechanical Behavior in Concrete Structure under External Sulfate Attack and Wetting–Drying Cycles. *Mater. Des.* **2024**, *241*, 112908. [CrossRef]
5. Sedaghatdoost, A.; Behfarnia, K. Mechanical Properties of Portland Cement Mortar Containing Multi-Walled Carbon Nanotubes at Elevated Temperatures. *Constr. Build. Mater.* **2018**, *176*, 482–489. [CrossRef]
6. Hassan, A.; Galal, S.; Hassan, A.; Salman, A. Utilization of Carbon Nanotubes and Steel Fibers to Improve the Mechanical Properties of Concrete Pavement. *Beni-Suef Univ. J. Basic. Appl. Sci.* **2022**, *11*, 121. Correction in *Beni-Suef Univ. J. Basic. Appl. Sci.* **2023**, *12*, 30. [CrossRef]
7. Chetty, K.; Watson, M.; Raine, T.; McGurgan, T.; Ladislaus, P.; Chen, J.; Zhang, S.; Lin, L.; Jiang, G. Enhancing Concrete and Mortar Properties and Durability Using Pristine Graphene Particles. *Coatings* **2022**, *12*, 1703. [CrossRef]
8. Prudente, I.N.R.; Santos, H.C.D.; Fonseca, J.L.; Oliveira, J.F.R.; Shibutani, A.B.; Gimenez, I.D.F.; Santos, E.A.D.; Barreto, L.S. Highlights on the Effects of Graphene-Family Materials Dispersion on Hydration and Mechanical Properties of Cement-Based Materials. *ACS Omega* **2025**, *10*, 55161–55184. [CrossRef] [PubMed]
9. Maqsood, S.; Ali, M.M.; Shittu, R.A.; Kim, T.-Y. Impact of Carbon Nanotubes on Chloride Diffusion in Cement Mortar under Temperature Gradient Conditions. *Sci. Rep.* **2025**, *15*, 19219. [CrossRef] [PubMed]
10. Arrechea, S.; Guerrero-Gutiérrez, E.M.A.; Velásquez, L.; Cardona, J.; Posadas, R.; Callejas, K.; Torres, S.; Díaz, R.; Barrientos, C.; García, E. Effect of Additions of Multiwall Carbon Nanotubes (MWCNT, MWCNT-COOH and MWCNT-Thiazol) in Mechanical Compression Properties of a Cement-Based Material. *Materialia* **2020**, *11*, 100739. [CrossRef]

11. Adhikary, S.K.; Rudžionis, Ž.; Rajapriya, R. The Effect of Carbon Nanotubes on the Flowability, Mechanical, Microstructural and Durability Properties of Cementitious Composite: An Overview. *Sustainability* **2020**, *12*, 8362. [CrossRef]
12. Zhou, Y.; Wang, Y.; Gao, T.; Ling, Y.; Jiang, N.; Tawfek, A.M.; Yuan, H. Optimization of Graphene Nanoplatelets Dispersion and Its Performance in Cement Mortars. *Materials* **2022**, *15*, 7308. [CrossRef] [PubMed]
13. Ge, Z.; Qin, J.; Sun, R.; Guan, Y.; Zhang, H.; Wang, Z. The Effect of the Addition of Graphene Nanoplatelets on the Selected Properties of Cementitious Composites. *Front. Built Environ.* **2021**, *7*, 673346. [CrossRef]
14. Khan, H.; Zahid, Z.B. Investigating the Structural Performance of Graphene Nanoparticles Infused Reinforced Concrete. *Discov. Civ. Eng.* **2025**, *2*, 52. [CrossRef]
15. Onaizi, A.M.; Amran, M.; Tang, W.; Betoush, N.; Alhassan, M.; Rashid, R.S.M.; Yasin, M.F.; Bayagoob, K.H.; Onaizi, S.A. Radiation-Shielding Concrete: A Review of Materials, Performance, and the Impact of Radiation on Concrete Properties. *J. Build. Eng.* **2024**, *97*, 110800. [CrossRef]
16. U.S. Nuclear Regulatory Commission. *A Review of the Effects of Radiation on Concrete in Nuclear Power Plants*; NUREG/CR-7171; U.S. Nuclear Regulatory Commission: Washington, DC, USA, 2013.
17. AlHamadi, F.I.; Shittu, R.A.; Sherief, M.; AlFantazi, A.; Alkaabi, A.K. Durability and Radiation Shielding Performance of Blended Cement Mortar under Increased Ambient Temperature and Sulfate Exposure in Arid Environments. *Sci. Rep.* **2025**, *16*, 922. [CrossRef] [PubMed]
18. Shittu, R.A.; AlHamadi, F.; Sherief, M.; AlFantazi, A.; Alkaabi, A.K. Factors Influencing the Radiation Shielding Capacity of Concrete Exposed to Aggressive Arid Environment: A Comprehensive Review. *Int. J. Concr. Struct. Mater.* **2025**, *19*, 91. [CrossRef]
19. Sherief, M.M.; Shittu, R.A.; Alhamadi, F.I.; Alkaabi, A.; Alfantazi, A. Concrete Durability in Arid Region: Influence of Seasonal Temperature and Humidity Variation on Sulfate Attack on Modified Cement Mortar. *Int. J. Concr. Struct. Mater.* **2026**, *20*, 44. [CrossRef]
20. *ASTM C109/C109M-24*; Standard Test Method for Compressive Strength of Hydraulic Cement Mortars (Using 50 mm [2 in.] Cube Specimens). ASTM International: West Conshohocken, PA, USA, 2024.
21. *ASTM C348-21*; Standard Test Method for Flexural Strength of Hydraulic-Cement Mortars. ASTM International: West Conshohocken, PA, USA, 2021.
22. *ASTM C597-22*; Standard Test Method for Ultrasonic Pulse Velocity Through Concrete. ASTM International: West Conshohocken, PA, USA, 2022.
23. *AASHTO T 358-24*; Standard Method of Test for Surface Resistivity Indication of Concrete's Ability to Resist Chloride Ion Penetration. American Association of State Highway and Transportation Officials: Washington, DC, USA, 2024.

Disclaimer/Publisher's Note: The statements, opinions and data contained in all publications are solely those of the individual author(s) and contributor(s) and not of MDPI and/or the editor(s). MDPI and/or the editor(s) disclaim responsibility for any injury to people or property resulting from any ideas, methods, instructions or products referred to in the content.